PACS numbers: 42.62.–b; 61.80.Ba
DOI: 10.1070/QE2011v041n07ABEH014420

Change in the surface morphology and chemical composition of some oxide crystals under UV laser irradiation

A.S. Kuzanyan, G.R. Badalyan, V.S. Kuzanyan,
V.R. Nikogosyan, S.Kh. Pilosyan, V.M. Nesterov

Abstract. **The effect of the 248-nm KrF and 355-nm YAG : Nd^{3+} laser radiation on the surface morphology and chemical composition of $SrTiO_3$, Sr_2RuO_4, $PbMoO_4$, $LiNbO_3$, $Y_3Al_5O_{12}$, and Al_2O_3 crystals has been studied. A relationship between the laser energy density on the sample surface and the surface roughness caused by the irradiation is determined. A technique for determining exactly the geometric surface characteristics is proposed. The effect of the surface roughness on the results of energy-dispersive X-ray (EDX) microanalysis has been investigated. A method for correcting the EDX data for samples with a rough surface has been developed. It is shown that the small variation in the composition of $PbMoO_4$, $LiNbO_3$, $Y_3Al_5O_{12}$, and Al_2O_3 samples after laser irradiation can be explained by the measurement error, related to the change in the surface roughness. At the same time, the irradiation of $SrTiO_3$ and Sr_2RuO_4 crystals by a YAG : Nd laser changes the chemical composition of their surface layers.**

Keywords: *laser processing, oxide crystals, surface morphology, chemical composition.*

1. Introduction

Immediately after the development of the ruby laser, it was used to investigate the interaction of high-power radiation with matter. In particular, the results of studying the interaction of laser radiation with the surfaces of solids [1, 2] and with liquids [3] and gases [4] were published in 1963. Currently lasers are applied in almost all fields of human activity. In particular, laser radiation is widely used to purposefully modify the microstructure and physical properties of solids: metals, alloys, semiconductors, and oxides. We will dwell on the interaction of laser radiation with the surface of some oxides.

Lithium niobate ($LiNbO_3$) is one of the most universal materials of integrated optics. Micromodification of its surface by laser radiation is a powerful tool, which expands greatly the range of application of $LiNbO_3$ crystals, in particular, as a base for microdiffraction elements and nonlinear photonic crystals [5]. Modification of the surface relief of lithium niobate crystals by nanosecond UV laser radiation was used to prepare micrometre and submicrometre lattices and Bragg reflectors [6, 7]. The main advantages of this method are the low contamination of the surface processed, high processing rate, and high spatial resolution. It was shown in [8] that the ablation threshold for $LiNbO_3$ crystals exposed to nanosecond UV radiation is lower than that for the femtosecond IR radiation. At the same time, an analysis of the Nd^{3+} microluminescence spectra revealed that nanosecond UV ablation leads to the formation of large concentration inhomogeneities and microstructural defects (dislocations, colour centres). However, no quantitative data on the change in the microstructure and chemical composition of $LiNbO_3$ crystals were reported in [8]. In our opinion, the character of these changes, induced by nanosecond UV radiation, must be refined.

The effect of excimer laser radiation on another multifunctional material – zinc oxide (ZnO) – was investigated in [9]. Scanning electron microscopy revealed the formation of zinc nanoparticles on the ZnO crystal surface.

Another field of application of UV laser radiation is the laser activation of oxide surfaces. Laser ablation of an oxide surface leads to the formation of catalytic centres on it, which can capture metal atoms from special solutions. The experimental data on the laser activation of the surface of Al_2O_3, ZrO_2, $LiNbO_3$, CeO_2, $SrTiO_3$, and other crystals were reviewed in [10]. These data concern basically the conditions for activating the insulator surface. It was suggested in [10] that the surface activation is accompanied by the formation of point defects (for example, F centres in Al_2O_3 and ZrO_2). However, no quantitative data on the change in the chemical composition of the surface of crystals studied were reported in [10].

Another interesting physical phenomenon, which can hardly be widely applied in practice without lasers, is the high-temperature superconductivity. The discovery of this phenomenon in cuprates initiated a search for oxide superconductors with even higher critical parameters. One of the ways for searching and fabricating new superconductors is to change the properties of materials by laser irradiation. Laser radiation can destroy superconductivity, form it in nonsuperconducting materials, improve the current-carrying properties, and increase the critical temperature of superconductors. Previously [11, 12] we showed that laser-

A.S. Kuzanyan, G.R. Badalyan, V.S. Kuzanyan, V.R. Nikogosyan
Institute of Physics Research, National Academy of Sciences of Armenia, 0203 Ashtarak, Armenia; e-mail: akuzan@ipr.sci.am;
S.Kh. Pilosyan, V.M. Nesterov P.N. Lebedev Physics Institute, Russian Academy of Sciences, Leninsky prosp. 53, Moscow, 119991 Russia; e-mail: s_pilosyan@mail.ru

Received 22 September 2010; revision received 22 April 2011
Kvantovaya Elektronika **41** (7) 619 – 625 (2011)
Translated by Yu.P. Sin'kov

irradiated Sr_2RuO_4 crystals possess new properties, which can be due to the superconductivity at temperatures of ~ 200 K. According to the data of energy-dispersive X-ray (EDX) microanalysis, the occurrence of these properties is accompanied by a possible change in the oxygen/ruthenium concentration ratio ([O]/[Ru]). It is important to explain this effect both to facilitate the search for the room superconductivity and to gain a deeper insight into the possibility of purposeful modification of the chemical composition and surface morphology of oxide crystals by laser radiation. We made such an attempt in [13]; however, only the qualitative estimates of the changes in the chemical composition of Sr_2RuO_4 under UV laser irradiation were reported.

The aforementioned data concern only a small part of possible applications of the laser modification of solid surfaces. At the same time, there are practically no quantitative data in the literature on the changes in the chemical composition of the surface of laser-irradiated samples. This is no surprise, because laser irradiation changes the properties of a thin surface layer. Therefore, one needs a method of microvolumetric chemical analysis to solve this problem. Such methods (rather sparse) include EDX microanalysis. Accurate quantitative EDX measurements require a maximally smooth sample surface; however, this condition is not satisfied in most cases of pulsed laser irradiation of materials.

The purposes of this study were as follows:

(i) to investigate the effect of UV laser radiation on the surface morphology and chemical composition for a number of oxide crystals;

(ii) to analyse the relationship between the EDX data and the surface roughness of oxide crystals, caused by both laser irradiation and mechanical treatment;

(iii) to propose a method for determining experimentally the chemical composition of rough surfaces, including the laser-ablated surfaces.

2. Experimental

2.1 Preparation of samples and analytical methods

We investigated three groups of samples of different oxides: L1, L2, and M. The samples of group L1 were irradiated by the third harmonic (355 nm) of a $YAG:Nd^{3+}$ laser. The energy density F on the sample surface reached 10^3 J cm^{-2}, the pulse width $\tau_{1/2}$ was 20 ns, and the pulse repetition rate was 30 Hz. The laser beam was focused on the sample surface into a spot 4 μm in diameter. The spot was scanned over the surface with a velocity of 20 μm s^{-1} to form an irradiated area 300×300 μm in size, which was used for further analysis. The samples of group L2 were irradiated by an excimer KrF laser in the single-pulse regime ($\lambda = 248$ nm, $F \leqslant 8$ J cm^{-2}, $\tau_{1/2} \leqslant 10$ ns). The laser beam was not scanned over the sample surface.

The short-wavelength absorption edge of most oxides is in the UV region. This fact determined the choice of the laser radiation wavelengths. The excimer laser energy was sufficient for ablation on areas of ~ 1 mm^2 in size, which made it possible to perform EDX microanalysis and profilometry. The radiation of the $YAG:Nd^{3+}$ laser was focused into a spot with a sufficiently small size to provide a high energy density on the samples without their destruction (because of the low energy per pulse). The $YAG:Nd^{3+}$ laser beam was scanned over the sample surface in order to (i) obtain a sufficient area for further study and (ii) form a striation surface structure, similar to that studied in [6, 7].

The samples of group M were treated by grinding powders to prepare surfaces of different roughness. Generally a mechanical treatment does not change the chemical composition of the sample surface; hence, the samples of this group can be considered as references of invariable composition but with different degrees of surface roughness.

The structure and chemical composition of the samples were analysed using a Vega TS 5130MM scanning electron microscope in combination with an INCA Energy 300 X-ray microanalyser. A semiconductor Si(Li) X-ray detector with a resolution of 126 eV (for the Mn K_α line) was used, which made it possible to detect all elements with atomic numbers larger than beryllium. The absolute statistical errors in measuring the concentration ratios of elements (in at %) were as follows: $\sigma([O]/[Ti]) = \pm 0.09$, $\sigma([O]/[Sr]) = \pm 0.11$ for $SrTiO_3$; $\sigma([O]/[Y]) = \pm 0.09$, $\sigma([O]/[Al]) = \pm 0.05$ for $Y_3Al_5O_{12}$; $\sigma([O]/[Al]) = \pm 0.09$ for Al_2O_3; $\sigma([O]/[Nb]) = \pm 0.05$ for $LiNbO_3$; $\sigma([O]/[Mo]) = \pm 0.15$, $\sigma([O]/[Pb]) = \pm 0.13$ for $PbMoO_4$; and $\sigma([O]/[Ru]) = \pm 0.13$, $\sigma([Sr]/[Ru]) = \pm 0.04$ for Sr_2RuO_4.

Laser radiation can change both the chemical composition of the samples and their surface roughness, which, in turn, affects the EDX results. In this ambiguous situation it is rather difficult to find out the nature of the changes in the physical properties within the 'physical property – laser irradiation – change in the physical property' chain. The effect of surface roughness on the EDX data in the approximation of saw-tooth surface profile was theoretically estimated in [14]. To calculate this effect, it is necessary to know the exact values of the arithmetic mean roughness amplitude R_a and the angle α, which characterises the saw-tooth profile. The roughness effect is determined by the correction coefficient R_Ω (the ratio of the measured element concentration to its real value).

The R_Ω value was calculated using the depth distribution of the generated characteristic X rays, with allowance for their reabsorption in the sample:

$$R_\Omega = 1 - (1 - R_{\Omega 0}) \exp[-Z_m \cot\psi/(4R_a \cot\alpha)], \qquad (1)$$

where ψ is the angle between the exit direction of the X rays emerging from the sample and the normal to the sample surface (in our system, $\psi = 45^\circ$); the quantity $R_{\Omega 0}$ takes into account the change in the characteristic X-ray intensity on a rough surface in the limiting case where the size Z_m of the emitting region is much smaller than the roughness period L.

The difficulties in calculating the correction coefficient stem from the fact that the parameters R_a and α have different values on different areas of the real surface.

2.2 Technique for determining the geometric surface characteristics

The sample surface profile was measured on an AMBI0S Technology XP-1 profilometer with a vertical resolution of 1.5 Å (for a height drop of no more than 10 μm) and a horizontal resolution of 100 nm. The profilometry was performed with the following scanning characteristics: the scan length $X = 300 - 1000$ μm, a tip pressure force of 0.05 mg, and a scanning rate of 0.01 – 0.05 mm s^{-1}.

The following parameters were chosen for the quantitative description of the surface profile:

(i) standard arithmetic mean roughness amplitude R_a for the surface area under consideration;

(ii) maximum (R_a^{max}) and minimum (R_a^{min}) arithmetic mean roughness amplitudes for the measurements on 100-μm-long surface portions;

(iii) arithmetic mean value of angle α for a surface portion, α_{aver};

(iv) fractions of scanned surface area (in percent) with tilt angles of $\alpha \leqslant 10^\circ$, 20°, and 30°;

(v) mean roughness depth D for the laser-processed area (samples of group L1).

The profilometer automatically calculates the arithmetic mean roughness amplitude for the area scanned. To determine the surface roughness with a higher accuracy, the scanned area was divided into portions 100 μm long, on which R_a values were measured. The data obtained were used to find R_a^{max} and R_a^{min}.

The angular surface characteristics were determined using the digital profilometry data: the coordinates of points on the scanned area of the sample surface (scan length X and relief height Y). For the portions corresponding to each profilometer step, the angle made by the sample surface portion with the horizontal plane was calculated from the formula $\alpha = \arctan[|Y_n - Y_{n-1}|(X_n - X_{n-1})^{-1}]$. The profilometer step n was chosen to be ~ 0.2 μm. Then all the angular data were input in the Origin program to plot the distribution histograms for angles α, and these histograms were used to calculate the fraction of the sample surface area corresponding to a certain range of angles α.

3. Experimental results and discussion

3.1 Surface morphology

Let us consider the surface morphology for the samples of the three groups under study by the example of strontium titanate crystals. Micrographs of the $SrTiO_3$ surface are shown in Fig. 1. It can be seen that the surfaces of the samples of groups L1 and L2 differ significantly, whereas the surfaces of the samples L2 and M have a similar structure. This is also evidenced by the surface profiles of the samples (Fig. 2). Valleys as deep as 2000 nm dominate on the surface of sample L1, whereas the surface profile of the sample L2 changes mainly within ±300 nm.

The dependence of the surface roughness amplitude for the samples L2 on the laser energy density is shown in Fig. 3. One can clearly see an increase in the roughness amplitude with an increase in the laser energy density, with a tendency to saturation.

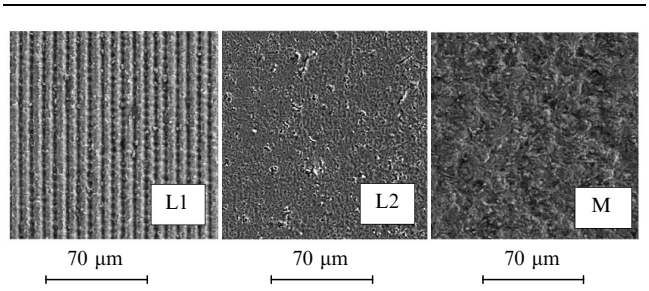

Figure 1. Microphotographs of the surfaces of the $SrTiO_3$ samples irradiated by YAG : Nd^{3+} and excimer KrF lasers (L1 and L2, respectively) and mechanically treated samples (M).

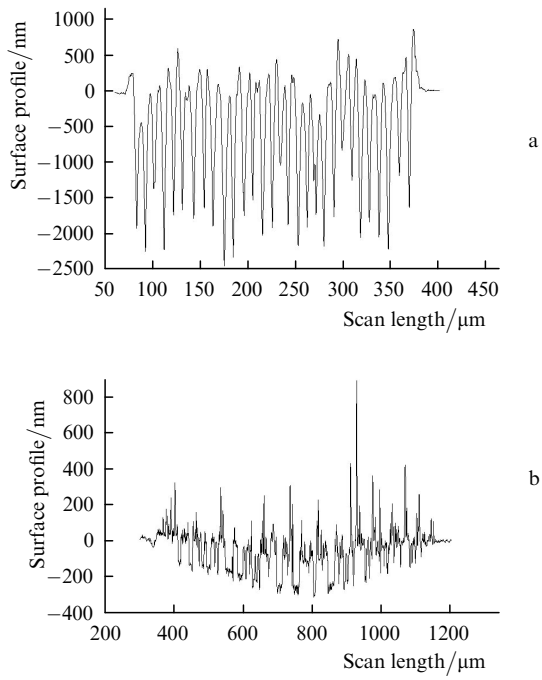

Figure 2. Surface profiles of the $SrTiO_3$ samples of groups (a) L1 and (b) L2.

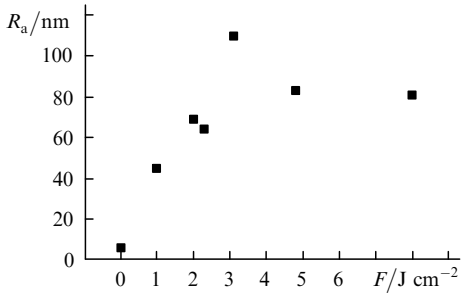

Figure 3. Dependence of the surface roughness amplitude R_a for the $SrTiO_3$ samples (L2) on the laser energy density F.

Consider more thoroughly the surface parameters of the mechanically treated $SrTiO_3$ samples. Table 1 contains the roughness parameters for several $SrTiO_3$ samples of group M. It can be seen that an increase in R_a increases the difference between R_a^{max} and R_a^{min} and reduces the fraction of the surface area corresponding to small angles α. However, even for the sample with the roughest surface ($R_a = 1853.5$ nm), the fraction of the surface area with $\alpha \leqslant 30^\circ$ exceeds 90 %. The distributions of small and large angles α are fairly uniform for both short and long scans (Fig. 4).

These regularities were also observed for the mechanically processed surfaces of $LiNbO_3$, $PbMoO_4$, $Y_3Al_5O_{12}$,

Table 1. Surface characteristics of the $SrTiO_3$ samples (M) according to the profilometry data.

Sample No.	R_a/ nm	R_a^{max}/ nm	R_a^{min}/ nm	α_{aver}/ deg	Fraction of the surface area (%) at different α		
					$\alpha \leqslant 10^\circ$	$\alpha \leqslant 20^\circ$	$\alpha \leqslant 30^\circ$
10	323.6	372.6	204.6	9.56	59.2	89.7	98.6
14	612	791	418	11.832	49.2	81.1	96.4
28	885	1095	605	13.38	45.0	75.1	92.7
4	1853	2563	983	14.939	37.5	69.9	90.9

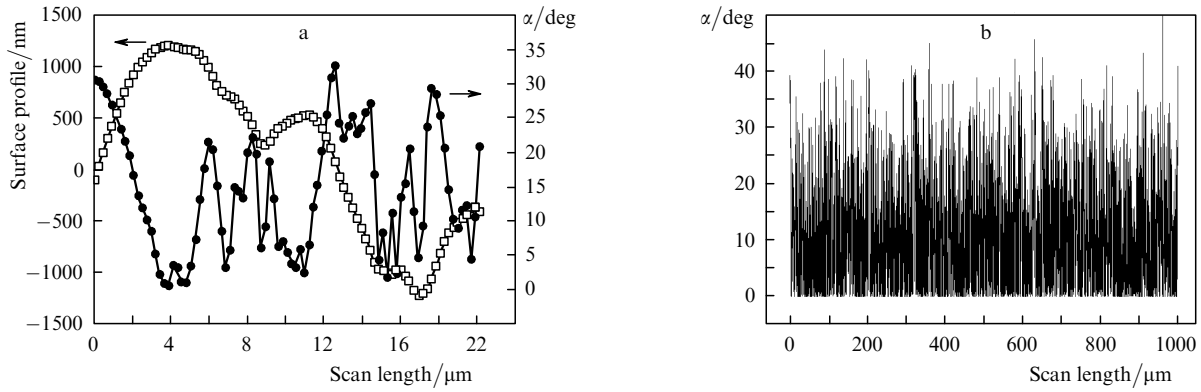

Figure 4. (a) Surface profile and the angle α for the mechanically treated $LiNbO_3$ sample at a profilometer scan length of 20 μm. (b) The angle α for the same sample at a scan length of 1000 μm.

and Al_2O_3 samples. These data, as well as the results for the samples of group L2, are omitted for brevity.

Let us now consider the surface characteristics of the samples of group L1 (Table 2). As can be seen in the table, the small-angle fraction is large for the $LiNbO_3$ samples and small for the $PbMoO_4$ samples. The yttrium–aluminum garnet samples, for which the parameter D is positive, differ significantly from the other samples (Fig. 5). Based on the data of Table 2, we can state that areas with small α values are also dominant on the surfaces of the samples L1.

3.2 Relationship between the surface roughness and the EDX data

The detailed data on the samples of group L2 are listed in Table 3. According to these results, the deviations from the exact stoichiometric ratio of oxygen and metal concen-

Table 2. Profilometry data for the samples of group L1.

Sample	Sample No.	X/μm	D/nm	R_a^{max}/nm	α_{aver}/deg	Fraction of the surface area (%) at different α				
						$\alpha \leqslant 10^\circ$	$\alpha \leqslant 20^\circ$	$\alpha \leqslant 30^\circ$	$\alpha \leqslant 40^\circ$	$\alpha \leqslant 50^\circ$
$PbMoO_4$	1	300	−4296	787	20.7	23	45.6	74.2	94.9	99.9
	2	300	−4104	1276	24.2	19.1	37	58.6	83.7	98.8
	3	300	−6266	1262	20.4	26	50.6	72.6	91.9	99.2
Sr_2RuO_4	1	400	−3610	900	8.06	68.9	92.4	98.2	99.87	
	2	100	−3421	1030	14.18	49	71	85	97	99.6
	3	100	−3656	561	7.98	74	95	97.5	100	
	4	200	−2729	424	10.24	54.2	85.8	96.3	100	
$LiNbO_3$	1	82	−1295	463	9.5	65	86	94.7	100	
	2	81	−1734	406	8.8	64	90	98.43	100	
	3	68	−1434	751	8.5	65	94	99	100	
$SrTiO_3$	1	250	−3070	1100	18.81	26.97	54.27	81.91	96.1	99.4
	2	300	−2437	901	22.66	23.8	44.4	70.2	92.8	99.5
	3	300	−1742	805	16.13	34.8	64.3	87.5	98.2	99.9
	4	300	−553	573	20.98	28.32	47.39	67.72	95.88	100
$Y_3Al_5O_{12}$	1	100	490	397	13.83	42.1	71.8	89.7	98.8	
	2	140	300	244	10.56	53.5	82.5	97.3	99.85	

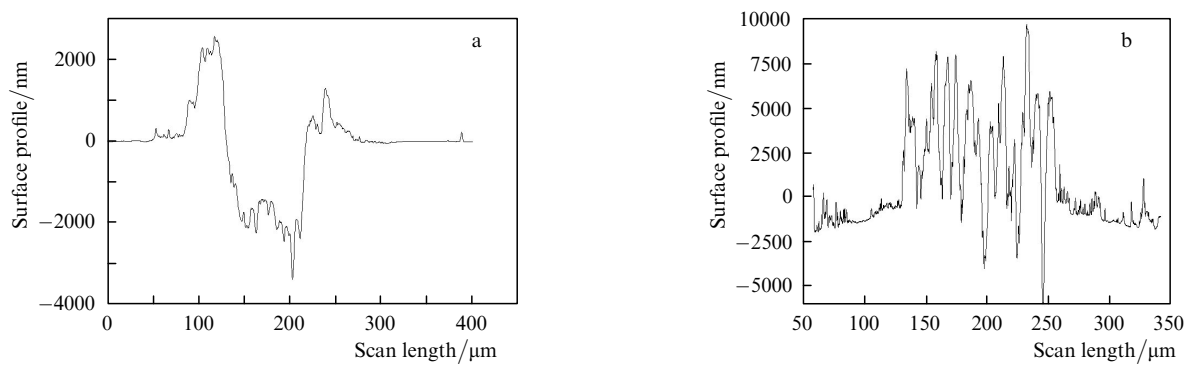

Figure 5. Surface profiles of the (a) $LiNbO_3$ and (b) $Y_3Al_5O_{12}$ samples (group L2).

Table 3. Conditions for obtaining an ablated spot and the EDX data on the $SrTiO_3$ samples (group L2).

Sample No.	E/mJ	S/mm^2	F/J cm^{-2}	R_a/nm	EDX data				
					[O] (at %)	[Ti] (at %)	[Sr] (at %)	[O]/[Ti]	[O]/[Sr]
1				6	60.15 ± 0.8	20.04 ± 0.3	19.81 ± 0.55	3 ± 0.09	3.04 ± 0.11
2	6	0.3	2	69	60.61	19.45	19.94	3.12	3.04
3	7.5	0.33	2.3	64	60.75	19.46	19.78	3.12	3.07
4	15	1.56	1	45	60.24	19.99	19.77	3.01	3.05
5	30 (5 pulses)	0.626	4.8	83	59.97	19.92	20.1	3.01	2.98
6	30	0.378	8	81	60.45	19.54	20.01	3.09	3.01
7	30	0.967	3.1	110	61.16	19.30	19.55	3.17	3.13

Note: E is the laser pulse energy, S is the irradiated area, and F is the energy density.

trations are within the measurement error even with the correction to the sample roughness disregarded. Note that this correction is small for the samples L2, because the R_a values obtained are small as well.

Figure 6 shows the EDX data for the $SrTiO_3$ samples of groups L1 and M, with different surface roughnesses. The samples of both groups exhibit an increase in the oxygen/metal concentration ratio with an in increase in R_a; with the same R_a values, this ratio is much larger for the samples of group L1. A question remains open: is the elevated oxygen/metal ratio for the $SrTiO_3$ samples of group L1 caused by a change in the geometric characteristics of the surface or is it due to some other factor?

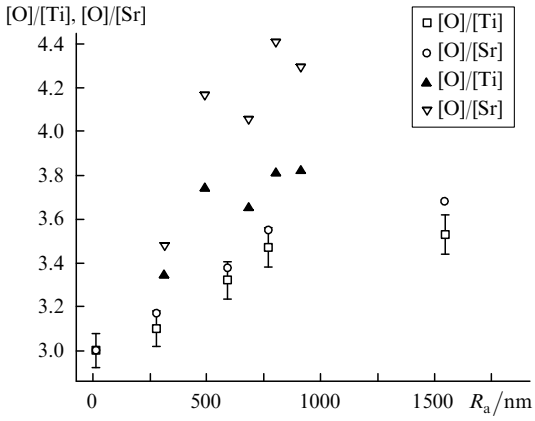

Figure 6. EDX data for the $SrTiO_3$ samples of groups (▲, ▽) L1 and (□, ○) L2, with different surface roughnesses.

In accordance with [14], we calculated the correction factors R_Ω for the oxygen/metal concentration ratios for $PbMoO_4$, $LiNbO_3$, $SrTiO_3$, $Y_3Al_5O_{12}$, Al_2O_3, and Sr_2RuO_4. As an example Fig. 7 shows the dependences of the correction factor R_Ω for the [O]/[Pb] ratio ($PbMoO_4$ crystal). One can see that the parameters $R_a = 1000$ nm and $\alpha = 40^\circ$ correspond to $R_\Omega = 1.3$. Thus, the [O]/[Pb] ratio determined by the EDX method for the $PbMoO_4$ sample with the aforementioned characteristics, may exceed the true value by almost a third because of the surface roughness. The dependence $R_\Omega(R_a, \alpha)$ is similar for the other crystals under study: R_Ω increases with an increase in R_a and α in all cases. Figure 8 shows the EDX data for the $LiNbO_3$ samples subjected to mechanical and laser treatments as an example of the effect the roughness has on the experimental values of the correction factor R_Ω. The R_Ω value for the [O]/[Nb] ratio in the samples of group M increases to 1.15

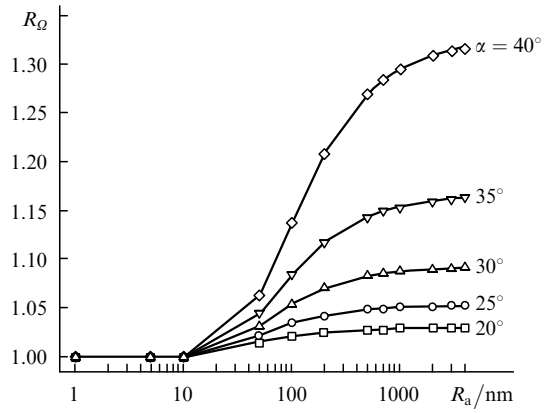

Figure 7. Dependences of the correction coefficient R_Ω for the [O]/[Pb] ratio ($PbMO_4$ crystal) on the surface roughness amplitude at different angles α.

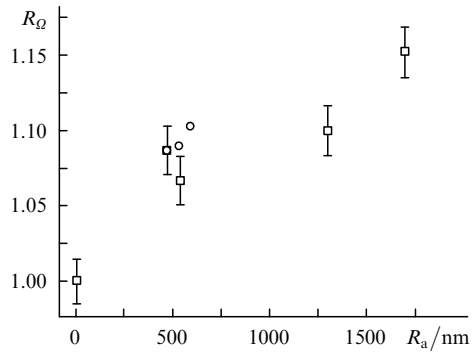

Figure 8. Dependences of the experimental values of the correction coefficient R_Ω for the [O]/[Nb] ratio on the surface roughness amplitude R_a for the $LiNbO_3$ samples of groups (○) L1 and (□) M.

with an increase in the roughness amplitude to 1500 nm. At identical roughness amplitudes the R_Ω value for the samples of group L1 slightly exceeds that for the samples M; however, this difference does not exceed the measurement error.

As was noted above, the correction factor depends also on the angle α; therefore, we will consider the method for calculating R_Ω taking into account this dependence. The entire range of angles α is divided into five ranges, each 10° wide. Table 4 contains the parameters corresponding to these ranges for one of the Sr_2RuO_4 samples: the correction factor R_Ω (the [O]/[Ru] ratio corresponding to the maximum angle in each range); the fractions of the sample surface area, S; and the contributions of the correction factor for

each range ($R_\Omega S$ product). The sum of the S values for all five angular ranges is unity. This means that the entire crystal surface is characterised by α values lying in the range of $0 < \alpha < 50^\circ$. Having summed the contributions $R_\Omega S$, we obtain the correction factor $R_\Omega^\Sigma = 1.029$ for the entire surface. Thus, because of the roughness of the sample with the aforementioned surface parameters, the true [O]/[Ru] ratio may differ from that measured by the EDX method by a factor of 1.029. The small difference of R_Ω^Σ from unity is an evident consequence of small S values for the surface areas with large angles α, for which R_Ω is also large.

Table 4. Calculation data on the correction coefficient R_Ω^Σ (Sr_2RuO_4 sample No. 59) for the [O]/[Ru] ratio ($R_a = 500$ nm).

α/deg	R_Ω (calculation)	Fraction S	$R_\Omega S$	R_Ω^Σ
0 – 10	1.009	0.697	0.703	
10 – 20	1.038	0.213	0.221	
20 – 30	1.107	0.064	0.071	1.029
30 – 40	1.285	0.024	0.031	
40 – 50	1.531	0.002	0.003	

Note that the data on R_Ω^Σ that are listed in Table 4 somewhat exceed the true values of the correction factor, since the calculations were carried out with the maximum R_Ω values for each angular range. To reduce the error in calculating R_Ω^Σ, one can use narrower ranges. However, the calculations showed that a decrease in the angular range from 10° to 1° only slightly changes the final result.

3.3 Change in the surface layer chemical composition

The R_Ω^Σ values for the samples of different oxides under study were calculated similarly. As an example, the calculated (R_Ω^Σ and experimentally found (R_Ω) values for the [O]/[Ru] (Sr_2RuO_4) and [O]/[Pb] ($PbMoO_4$) ratios are listed in Table 5. The bolded R_Ω values for two Sr_2RuO_4 samples of group L1 (with allowance for the absolute error) exceed greatly the calculated R_Ω for the [O]/[Ru] ratio (the same samples). This means that the increase in the [O]/[Ru] ratio as a result of the laser irradiation cannot be due to the change in the sample surface roughness. For the Sr_2RuO_4 samples of group M with similar roughness amplitudes, as well as for the $PbMoO_4$ samples, the difference between R_Ω and R_Ω^Σ is within the absolute measurement error, which is ± 0.13 for the [O]/[Ru] and [O]/[Pb] ratios. The laser-induced changes in the [O]/[Al] ratio for Al_2O_3 and $Y_3Al_{15}O_{12}$ and the [O]/[Nb] ratio for $LiNbO_3$ are also within the absolute error.

Table 5. Calculated (R_Ω^Σ) and experimental (R_Ω) correction coefficients for the [O]/[Ru] (Sr_2RuO_4) and [O]/[Pb] ($PbMO_4$) ratios.

Sample	Sample No.	Group	R_a	R_Ω^Σ	R_Ω
Sr_2RuO_4	57-1	M	260	1.015	1.056
	59	M	500	1.029	1.09
	57-2	M	600	1.024	1.013
	41-2	L1	500	1.027	**1.24**
	59 cl (II)	L1	700	1.04	**1.75**
$PbMoO_4$	10	M	530	1.023	1.065
	28	M	1400	1.04	1.081
	4	M	1940	1.267	1.053
	Air 2-1	L1	950	1.222	1.145
	Air 2-2	L1	1280	1.23	1.24

The very high complexity and peculiarity of the ruthenium chemistry is due to the fact that it readily passes from one valence state to another and has many valence states (from 0 to +8). The most stable ruthenium valence is +4 (RuO_2, Sr_2RuO_4). However, even in the oxide compounds (which are most interesting for us) ruthenium may have even a higher valence. For example, the ruthenium valence is +5 in $Sr_4Ru_2O_9$; +6 and +7 in, respectively, $M_2(RuO_4)$ and $M(RuO_4)$ (M is a monovalent metal); and, finally, +8 in RuO_4 [15, 16]. Based on the EDX data and proceeding from the electroneutrality principle, we can suggest that the valence of ruthenium ions in the surface layer of the Sr_2RuO_4 samples irradiated by the YAG : Nd laser reaches +7. This is a possible cause of the HTSC-like anomalies in the conductivity of Sr_2RuO_4 crystals at temperatures above 200 K [11, 12].

The calculations according to [14] show that the [O]/[Ti] and [O]/[Sr] ratios for a $SrTiO_3$ crystal with $R_a = 1000$ nm may increase by factors of 1.2 and 1.3, respectively. As can be seen in Fig. 6, the difference in the [O]/[Ti] and [O]/[Sr] ratios for mechanically treated samples is within the roughness correction. However, for the samples of group L1 the increase in the oxygen/metal concentration ratio exceeds the roughness-induced increase. This distinction is especially pronounced for the [O]/[Sr] ratio. The increase in the [O]/[Ti] ratio is comparable with the total correction, which is determined by the measurement error and the sample roughness, whereas for the [O]/[Sr] ratio this does not hold true. The large [O]/[Sr] ratio in the samples of group L1 is most likely to be caused by decrease in the Sr concentration in the surface layer of these samples, i.e., by the deviation from the $SrTiO_3$ stoichiometry as a result of the more intense strontium evaporation under laser irradiation.

4. Conclusions

The purposes of our study were reached by analysing the experimental data obtained by the EDX and profilometry methods, applying a theoretical model describing a saw-tooth surface profile. Based on this approach, we propose a method for determining the chemical composition of rough surfaces, to which laser-ablated surfaces belong. The practical importance of our study is specifically in the development of this method.

The results obtained can be generalised as follows.

(i) The relationship between the energy density of excimer laser ($\lambda = 248$ nm) and the surface roughness caused by the laser irradiation was established. A pronounced increase in the arithmetic mean roughness amplitude R_a to 100 nm with an increase in the laser energy density to 8 J cm^{-2} was observed.

(ii) A way for taking into account the effect of the surface roughness on the EDX data, based on the use of the exact values of the parameters characterising the sample surface, was proposed.

(iii) It was proven that the EDX data on the laser-irradiated Sr_2RuO_4 samples cannot be explained by the change in the surface roughness. These samples exhibited a significant increase in the oxygen content.

(iv) It was shown that the irradiation of the $SrTiO_3$ crystal surface by the third harmonic of a YAG : Nd^{3+} laser with an energy density of 10^3 J cm^{-2} changes the surface layer stoichiometry, whereas in the samples irradiated by an

excimer laser these changes were absent. Evidently, this result is due to the significant differences in the energy densities of these two lasers.

(v) The changes in the composition of the $PbMO_4$, $LiNbO_3$, $Y_3Al_5O_{12}$, and Al_2O_3 samples after their irradiation by both excimer and YAG : Nd^{3+} lasers are within the absolute experimental error.

The results obtained can be used both to study the effect of laser radiation on various materials (oxides, semiconductors, alloys, etc.), in particular, to purposefully search for materials with new physical properties, and to solve various technological problems, for example, to fabricate microdiffraction elements and nonlinear photonic crystals.

Acknowledgements. We are grateful to A.Z. Grasyuk for the attention to our study and fruitful discussions.

References

1. Ready J.F. *Appl. Phys. Lett.*, **3**, 11 (1963).
2. White R.M. *J. Appl. Phys.*, **34**, 3559 (1963).
3. Askar'yan G.A., Prokhorov A.M., Chanturiya G.F., Shipulo G.P. *Zh. Eksp. Tekh. Fiz.*, **17**, 2180 (1963).
4. Meyerand R.G., Haught A.F. *Phys. Rev. Lett.*, **9**, 403 (1963).
5. Capmany J., Fernández-Pousa C.R., Diéguez E., Bermúdez V. *Appl. Phys. Lett.*, **83**, 5145 (2003).
6. Wu B., Chu P.L., et al. Z. *IEEE J. Quantum Electron.*, **35**, 1369 (1999).
7. Chen K., Ihlemann J., Simon P., Baumann I., Sohler W. *Appl. Phys. A*, **65**, 517 (1997).
8. Rodenas A., Jaque D., Molpeceres C., Lauzurica S., Ocana J.L., Torchia G.A., Agullo-Rueda F. *Appl. Phys. A*, **87**, 87 (2007).
9. Khan E., Langford S, Dickinson J.T. *SPIE Newsroom*, 10.1117/2.1200906.1660 (2009).
10. Shafeev G.A. *Kvantovaya Elektron.*, **24**, 1137 (1997) [*Quantum Electron.*, **27**, 1117 (1997)].
11. Gulian A.M., Wood K.S., Van Vechten D., Claassen J., Soulen R.J., Qadri S., Osofsky M., Lucarelli A., Luepke G., Badalyan G.R., Kuzanyan V.S., Kuzanyan A.S., Nikoghosyan V.R. Cond-mat./0509313(2005).
12. Gulian A.M., Nikoghosyan V R., Van Vechten D., Wood K.S. *J. Contemporary Phys. (Armen. Acad. Sci.)*, **42**, 298 (2007).
13. Badalyan G.R., Petrosyan V.A., Nikoghosyan V.R., Petrosyan S.I., Kuzanyan A.S., Kuzanyan V.S., Gulian A.M. *J. Contemporary Phys. (Armen. Acad. Sci.)*, **46**, 40 (2011).
14. Yamada A., Fons P.J., Sakurai K., Matsubara K., Iwata K., Niki Sh. *J. Appl. Phys.*, **42**, 5811 (2003).
15. Chmielowski R., Madigou V., Blicharski M., Leroux Ch. *J. Cryst. Growth*, **310**, 3854 (2008).
16. Griffith W.P. *Found Chem.*, **12**, 17 (2010).